frontiers | Frontiers in Photonics

TYPE Original Research
PUBLISHED 08 December 2022
DOI 10.3389/fphot.2022.1019552



OPEN ACCESS

EDITED BY
Ben Sherlock,
University of Exeter, United Kingdom

REVIEWED BY
Shengnan Liu,
Erasmus Medical Center, Netherlands
Massimo Salvi,
Polytechnic University of Turin, Italy

*CORRESPONDENCE
Shengxian Tu,
sxtu@sjtu.edu.cn

SPECIALTY SECTION
This article was submitted to Biophotonics, a section of the journal Frontiers in Photonics

RECEIVED 15 August 2022
ACCEPTED 28 November 2022
PUBLISHED 08 December 2022

CITATION
Huang J, Ninomiya K, Tu S, Masuda S, Dijkstra J, Chu M, Ding D, Hynes SO, O'Leary N, Wijns W, Onuma Y and Serruys PW (2022), Calcified plaque detected on OCT with deep learning and cross-validated with optical and ultrasound signals: A complementary appraisal and preamble to combined IVUS-OCT catheter.
*Front. Photonics* 3:1019552.
doi: 10.3389/fphot.2022.1019552



# Calcified plaque detected on OCT with deep learning and cross-validated with optical and ultrasound signals: A complementary appraisal and preamble to combined IVUS-OCT catheter

Jiayue Huang[1], Kai Ninomiya[2], Shengxian Tu[3]*, Shinichiro Masuda[2], Jouke Dijkstra[4], Miao Chu[3], Daixin Ding[1], Sean O. Hynes[5], Neil O'Leary[2], William Wijns[1], Yoshinobu Onuma[2] and Patrick W. Serruys[2,6]

[1]The Lambe Institute for Translational Medicine and CÚRAM, University of Galway, Galway, Ireland, [2]Department of Cardiology, University of Galway, Galway, Ireland, [3]Biomedical Instrument Institute, School of Biomedical Engineering, Shanghai Jiao Tong University, Shanghai, China, [4]Division of Image Processing, Department of Radiology, Leiden University Medical Center, Leiden, Netherlands, [5]Department of Histopathology, University Hospital Galway and University of Galway, Galway, Ireland, [6]National Heart and Lung Institute, Imperial College London, London, United Kingdom

**Background:** The optical coherence tomography (OCT)-deep learning (DL) emerged as a promising tool for automated plaque characterization. However, its findings have not been compared with optical and ultrasound signals.

**Objectives:** The objective was to cross-validate the calcified plaque detected by OCT-DL, using comprehensive tissue characterization technologies including OCT-derived optical properties, intravascular ultrasound (IVUS)-virtual histology (VH) and echogenicity.

**Methods:** Five years after bioresorbable scaffold (BRS) implantation, 15 patients underwent OCT and IVUS imaging. The unique platinum markers in BRS facilitated precise OCT-IVUS co-registration. Calcified plaque detected by OCT-DL were corroborated by/with optical properties, greyscale (GS)-IVUS, IVUS-VH and echogenicity. The concordance between OCT-DL and other modalities was assessed by kappa statistics. The calcium arc measured by different modalities were compared by orthogonal linear regression.

**Results:** Forty-three calcified plaques were detected by DL in 72 matched anatomic slices, 41 (95%) were confirmed as pure (n = 29) or hybrid calcified plaque (n = 12) by optical properties. Weighted kappa between OCT-DL and GS-IVUS, IVUS-VH and echogenicity were 0.69, 0.60 and 0.60, respectively. After having excluded artifactual optical shadowing (n = 5) generated by guidewire or platinum marker, kappa increased to 0.77, 0.68 and 0.69, with agreement ranging between 90% and 93%. Calcium arc derived from OCT-DL

showed moderate correlation and agreement with GS-IVUS (ICCa = 0.81, difference = 1.73 ± 15.25°), IVUS-VH (ICCa = 0.69, difference = -5.60 ± 21.19°) and echogenicity (ICCa = 0.65, difference = 10.28 ± 18.70°).

**Conclusion:** OCT empowered by deep learning showed substantial agreement with optical and ultrasound signals. The comprehensive assessment provided by OCT and IVUS heralds the potential diagnostic value of combined IVUS-OCT catheters.

KEYWORDS

**optical coherence tomogaphy, intravascular ultrasound, deep learning, calcified plaque, bioresorbable scaffold**

# 1 Introduction

Coronary calcification has long been recognized as a predictor for future cardiac events. Its accumulation occurs concomitantly with the progression of atherosclerosis (Otsuka et al., 2014; Jinnouchi et al., 2020). The identification and quantification of calcified plaque can be well achieved *in-vivo* with intravascular ultrasound (IVUS) and optical coherence tomography (OCT).

IVUS enables the visualization of the entire vessel structure, making this imaging modality suitable for detecting both superficial and deep calcified plaque. Compared to IVUS, OCT has a higher resolution enabling detailed calcified plaque delineation and quantification. However, the limited tissue penetration of infrared light might preclude the accurate detection of deep calcified plaque.

Several technologies have been developed and validated with histology to make better interpretations of intracoronary images (Garcia-Garcia et al., 2011). IVUS-virtual histology (VH) performs spectral analysis of radio-frequency signals and classifies tissue into four major components (Nair et al., 2002). IVUS-based echogenicity refers to the mean grey-level of adventitia to discriminate hypo- and hyperechogenic tissues (Bruining et al., 2007). For OCT images, the optical properties such as attenuation and backscattering have been proven by histology to have the potential for differentiating different tissue types (Xu et al., 2008; van Soest et al., 2010; Liu et al., 2017; Teo et al., 2017). Multiple algorithms have also been proposed for an enhanced interpretation of OCT images (Athanasiou et al., 2014; Villiger et al., 2018; Prabhu et al., 2019; Lee et al., 2020), most of which have been restricted to differentiable tissue types, with the exception of cholesterol and foam cells. A fully automated plaque characterization algorithm based on deep convolutional network was recently developed and validated using the annotations by an expert panel, and OCT-DL showed an accuracy of 88.5% for delineating calcified plaque in OCT images (Chu et al., 2021). However, it has not been comprehensively cross-validated using optical and ultrasound signals.

The objective of the present study was to cross-validate the calcified plaque detected on OCT with deep learning (DL), using comprehensive tissue characterization technologies including OCT-derived optical properties, IVUS-VH and echogenicity on accurately aligned *in-vivo* imaging of human coronary arteries scaffolded with bioresorbable devices implanted 5 years earlier.

# 2 Materials and methods

## 2.1 Study design and materials

In ABSORB Cohort B trial (NCT00856856), baseline and 5-year follow-up frequency-domain OCT, greyscale (GS)-IVUS and IVUS-VH were acquired in 15 patients who have been implanted at baseline with the second generation of Absorb bioresorbable vascular scaffold (BRS) (Abbott Vascular, Santa Clara, CA, United States), where two pairs of 244 μm platinum markers were embedded in the struts at the proximal and distal ends to aid in deployment and visualization (Serruys et al., 2010).

In current study, we analyzed the 5-year follow-up imaging data. The scaffolds have been fully absorbed and the struts no longer hamper the visualization of calcified plaques. DL-based OCT plaque characterization, OCT attenuation and backscattering analysis, and GS-IVUS echogenicity analysis were performed, together with the IVUS-VH results, providing a comprehensive assessment of calcified plaques. The study protocol conforms to the ethical guidelines of the 1975 Declaration of Helsinki as reflected in a prior approval by the institution's human research committee. The ethics committee at each participating institution approved the protocol, and each patient gave written informed consent before inclusion.

## 2.2 OCT and IVUS acquisition

IVUS and OCT images were obtained using 20-MHz, phased-array IVUS catheters with an electronic rotation of 30 frames/second and C7/C8 frequency domain systems with a mechanic rotation of either 100 or 180 frames/second, respectively (Zeng et al., 2017; Zeng et al., 2018). IVUS-VH

was assessed at the gated end-diastolic phase, and its corresponding GS-IVUS images were analyzed for echogenicity.

## 2.3 Co-localization of OCT and IVUS cross-sections

The co-registration between OCT, GS-IVUS and IVUS-VH was achieved manually (Zeng et al., 2017; Zeng et al., 2018) utilizing the presence of endoluminal platinum markers located at the proximal and distal ends of the BRS, and common anatomic landmarks such as side branch, vein, pericardium, position and configuration of calcified plaque, characteristic lumen shape and circumferential profile of plaque thickness, and/or positional or directional relationship among all these landmarks. The matched OCT and IVUS were reviewed by an expert panel of five experienced cardiologists (Zeng et al., 2017; Zeng et al., 2018). IVUS-VH was regarded as the limiting factor for the number of matched cross-sectional images since it was only acquired at end-diastole. Nevertheless, the reproducible and precise co-registration performed by multiple experienced cardiologists remains the main asset of the present material.

## 2.4 Longitudinal window for OCT and IVUS

The pitch between consecutive OCT cross-sections was 0.1 mm or 0.2 mm. The pitch between consecutive IVUS cross-sections was around 0.5 mm, depending on patient's heart rate. In addition, the potential impact of oblique imaging, i.e., the imaging catheter positioned obliquely inside the lumen, during separate pullbacks is also not negligible. Thus, a longitudinal window of 0.4 mm was found reasonable for OCT images. More specifically, one or two cross-sections proximal and distal to the index cross-section were also investigated in OCT pullbacks with slice thickness of 0.2 mm or 0.1 mm, respectively.

## 2.5 OCT and IVUS analyses

The analyses of all matched OCT and IVUS cross-sections were performed at an academic core laboratory (Corrib Core Lab, University of Galway, Ireland). OCT images were analyzed by two experienced analysts (J.H. and K.N.), using the DL-based method and optical properties-based method, respectively. Echogenicity analysis was performed by another experienced analyst (S.M.), who was blind to the results of OCT analyses.

### 2.5.1 DL-based OCT analysis

The lumen contour, plaque compositions and media contour of each OCT pullback were automatically delineated using a recently developed software package (OctPlus, Pulse Medical Imaging Technology, Shanghai, China) (Chu et al., 2021). The plaque composition was characterized as fibrotic, lipidic or calcified, and biomarkers such as macrophage and cholesterol crystals were identified. Additional details about the DL algorithm could be found in Supplementary Methods. After DL analysis, the results of the selected cross-sections were recorded for further comparison.

### 2.5.2 Optical properties-based OCT analysis

The optical properties were analyzed using a customized and dedicated offline software (QCU-CMS, Leiden University Medical Center, Leiden, Netherlands). The lumen and external elastic membrane contour were detected semi-automatically, followed by the automatic computation of attenuation and backscattering coefficients.

In the initial study of Liu et al. (2017), the gold standard for OCT images was derived from *ex-vivo* glutaraldehyde fixed human coronary specimen. The various histological plaques were delineated and categorized by pathologists, who were unaware of the imaging results (Liu et al., 2017). Therefore the *in-vivo* calcified plaque identified by DL was considered as the new modality of imaging that was not validated directly against human coronary histology, but could indirectly be validated with other *in-vivo* imaging relying either on ultrasound or optical derived parameters that had been previously corroborated by histomorphometry (Nair et al., 2002; Bruining et al., 2007; Liu et al., 2017).

The delineation of the calcified plaques derived from DL served as regions of interest (ROI) for the optical properties-based analysis. More specifically, the OCT images with calcified plaque delineation from DL were superimposed to the QCU-CMS software with a transparency of 30%–50% for ROI delineation, thus ensuring the identical ROI between two different software. After ROI delineation, the optical properties including light attenuation and backscattering within each ROI were exported from QCU-CMS using the DataCollector software (Leiden University Medical Center, Leiden, the Netherlands) for further analyses.

### 2.5.3 IVUS analyses

IVUS-VH has been previously analyzed (Zeng et al., 2017) and revisited using QCU-CMS 32-bit version. The echogenicity analysis was performed using QCU-CMS 64-bit version. Five tissue types in vessel wall were automatically classified: calcified, hyperechogenic, upper-echogenic, hypoechogenic, and unknown (Bruining et al., 2007; Zeng et al., 2017). The subsets of upper-echogenic and unknown were created to exclude all matters in the dataset that do not account for regular tissue.

## 2.6 Cross-validation of calcified plaque

Considering the complexity of coronary calcification, instead of treating it as a binary "all-or-none" variable, we subdivided the OCT ROIs as pure, when calcification was the only tissue inside the ROI, hybrid calcified plaque, when there were additional tissue components inside the ROI, or non-calcified plaque when there was no calcification inside the ROI, depending on the numerical distribution of the optical properties (Liu et al., 2017). Details about the optical properties-based ROI validation are described in Supplementary Methods and Supplementary Figure S1.

For GS-IVUS, IVUS-VH and echogenicity, the binary identification of calcified plaque was retained (Zeng et al., 2017; Zeng et al., 2018). For GS-IVUS, the calcified plaque was identified as an echo-dense area with acoustic shadow behind (Mintz et al., 2001; Zeng et al., 2017; Zeng et al., 2018). Calcified plaque in IVUS-VH was detected as the confluent white-color area exceeding 0.0625 $mm^2$. For echogenicity, the area with grey-level intensity higher than adventitia and accompanied by an acoustic shadow was recognized as calcified plaque (Zeng et al., 2017).

## 2.7 Calcified plaque quantifications

The calcified plaque detected in different image modalities was automatically or semi-automatically quantified according to consensus (Mintz et al., 2001).

In OCT images, the calcified plaque was automatically quantified in OctPlus software. The arc of each plaque was obtained by positioning a protractor centered on the gravitational center of the lumen (Supplementary Figure S2A). In case the lateral part of the plaque was shadowed by guidewire artifact, it was excluded from calcium arc comparison with ultrasonic modalities.

For GS-IVUS, IVUS-VH and echogenicity, the calcium arc was manually measured using the same method as for OCT. The acoustic shadow in GS-IVUS, the area color-coded in white in IVUS-VH, and the calcium leading edge accompanied by an acoustic shadow in echogenicity were measured (Supplementary Figure S2B–D) and compared with OCT-derived calcium arc.

## 2.8 Statistical analysis

Continuous variables are reported as mean ± standard deviation or median (quartiles) as appropriate, while categorical variables are presented as counts (percentages). The difference between groups was tested using independent sample *t*-test, Mann-Whitney test or One-way Analysis of Variance (ANOVA), as appropriate. Paired *t*-test, Wilcoxon signed-rank test or repeated measures ANOVA were used for pair-wise comparison, as appropriate. The agreements between different imaging modalities were calculated using linear weighted kappa. Given the clustered nature of the current dataset, the bootstrap approach was applied with 500 replications, using the patient as cluster (Efron and Tibshirani, 1994). The bias-corrected 95% confidence interval (CI) was reported for the above-mentioned statistical results. Statistical assessments were performed with SPSS version 27.0.1.0 (SPSS Inc., Chicago, Illinois) and Stata SE version 15.0 (College Station, Texas). A 2-sided value of $p < 0.05$ was considered to be statistically significant.

# 3 Results

## 3.1 Study population

Seventy-two co-registered OCT and IVUS cross-sections from 15 patients were included in the present study. Supplementary Table S1 presents the baseline clinical characteristics.

## 3.2 Detection of calcified plaque

Figure 1 and Supplementary Figure S3 show two representative examples of the calcified plaque detected by optical and ultrasound signals. The DL delineated calcified plaques were further identified and classified as pure (Figures 1F–I) or hybrid calcified plaque (Supplementary Figure S3F–I) by optical properties.

The detection of calcified plaque by the five different modalities is presented in Figure 2. A total of 43 calcified plaques from 72 anatomical slices were detected by OCT-DL, among which 41 (95%) calcified plaques were further validated by optical properties. Twenty-nine (71%) of these validated ROIs were classified as pure calcified plaque, and 12 (29%) as hybrid calcified plaque. In GS-IVUS, 46 calcified plaques were identified, 37 (80%) of which were also identified by OCT-DL. Fifty and 42 calcified plaques were detected in IVUS-VH and echogenicity, respectively.

Discordances between optical and ultrasound signals were observed in 13 instances. Four calcified plaques were identified by OCT-DL algorithm and corroborated by optical properties, but not by ultrasound signals. Nine calcified plaques were detected by all the three ultrasonic modalities, but not identified by OCT-DL. The potential explanations for the discordances are presented in Figure 3. For five ultrasound signal-detected calcified plaques, their corresponding area in OCT were not imaged by optical signal due to the impact of guidewire artifact (Figures 3B1–B4) or the shadow created by the previously implanted endoluminal platinum marker (Figure 3C). Three IVUS-detected calcified plaques were "missed" by OCT possibly due to the limited

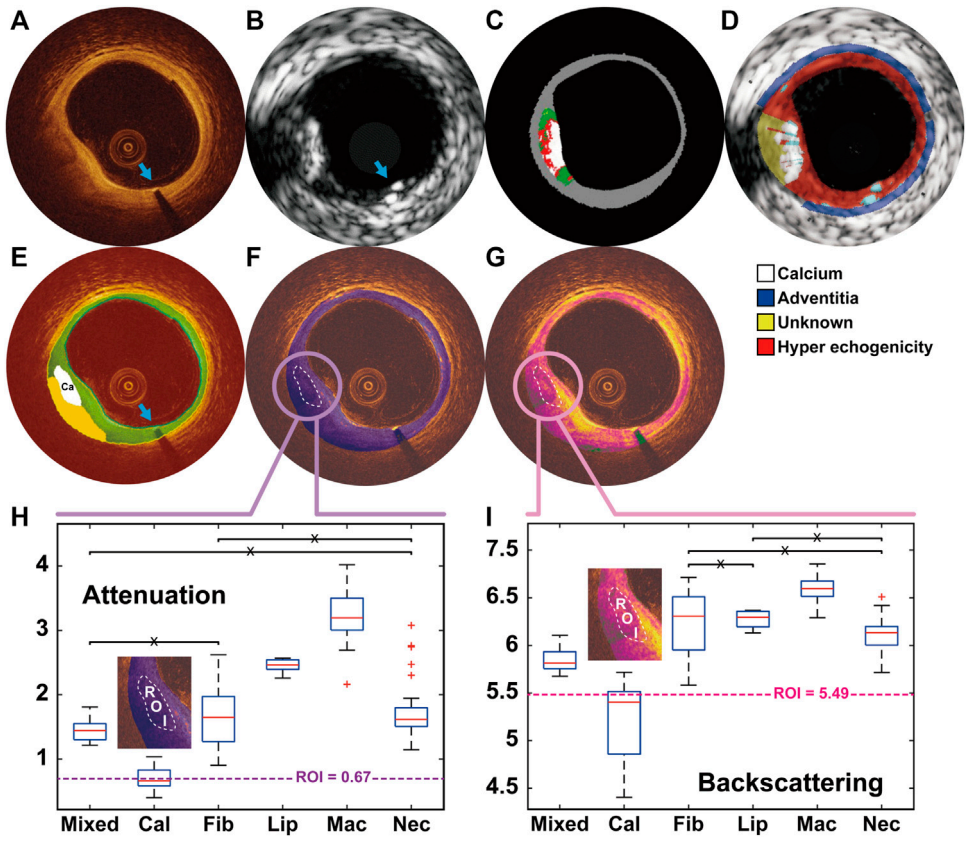


FIGURE 1
A representative example showing the calcified plaque detected in OCT and IVUS, and further classified as pure calcified plaque by the optical properties OCT **(A)** and IVUS **(B)** images were co-registered based on the presence of the previously implanted endoluminal platinum marker (blue arrows). Calcified plaque at 7–9 o'clock was detected by VH **(C)**, echogenicity **(D)** and OCT-DL algorithm **(E)**. The contour of DL detected calcified plaque were set as the region of interest (ROI) for the analysis of OCT attenuation **(F)** and backscattering **(G)**. By comparing the median values of the optical properties within ROI with the numerical results from histological studies **(H–I)**, the plaque was further classified as pure calcified plaque. DL: deep learning; IVUS: intravascular ultrasound; OCT: optical coherence tomography; VH: virtual histology.

penetration depth of infrared (Figures 3E1–E3). No specific reason could be found for one discordance (Figure 3D). An agreement among all modalities for the absence of calcified plaque was observed in 24 matched anatomic slices.

## 3.3 Concordance between OCT-DL and ultrasound signal

The concordance between OCT-DL and ultrasound signal in calcified plaque identification is presented in Table 1. For the whole series of 72 anatomic slices, the agreement between OCT-DL and GS-IVUS, IVUS-VH and echogenicity for calcified plaque detection were 90%, 87% and 87%, with weighted kappa being 0.69, 0.60 and 0.60 (Supplementary Table S2), respectively. After excluding the five cases where the corresponding areas of IVUS-detected calcified plaques in OCT were not imaged by the light beam, the agreement improved to 93%, 90% and 90%, with weighted kappa being 0.77, 0.68 and 0.69 (Supplementary Table S3), respectively.

## 3.4 Calcium arc comparison

The concordance between the calcium arc measured by OCT-DL and the measurement obtained from three ultrasound imaging modalities are presented in Supplementary Table S4 and Figure 4. Eight calcified plaques were excluded from calcium arc comparison since part of the plaque were hidden behind the OCT guidewire shadowing, resulting in 29 calcified plaques appropriately imaged for paired comparison with GS-IVUS and IVUS-VH. For calcium arc measured in echogenicity, 25 calcified plaques were included for paired comparison.

Good correlation and agreement were observed between the calcium arc measured by OCT-DL and GS-IVUS [ICCa = 0.81

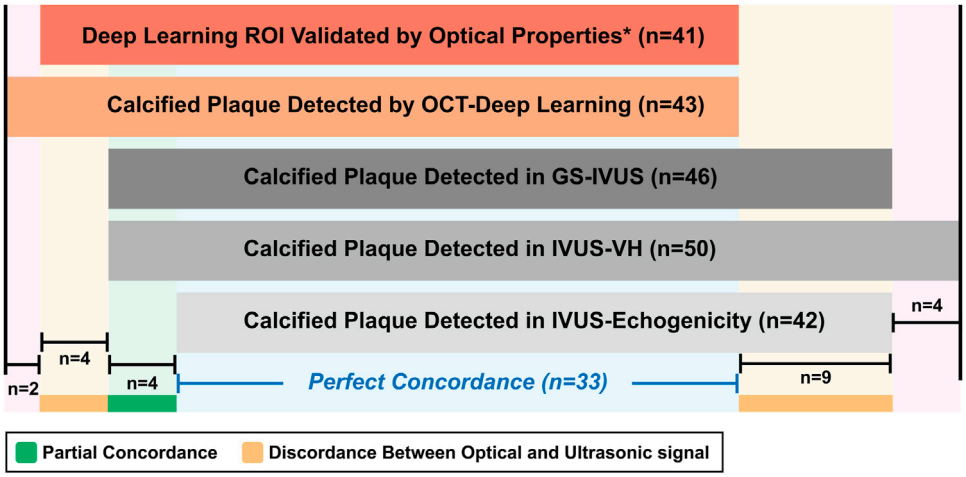


FIGURE 2
The detection of calcified plaques by OCT-DL, optical properties and ultrasound signals. * In present study, the optical properties-based OCT analysis was only performed when OCT-DL detected a calcified plaque. GS: greyscale. Other abbreviations as in Figure 1.

(95% CI: 0.68–0.91), difference = 1.73 ± 15.25°], while the concordance rates were moderate when comparing the calcium arc derived from OCT-DL with that measured in IVUS-VH [ICCa = 0.69 (95% CI: 0.54–0.81), difference = -5.60 ± 21.19°] and echogenicity [ICCa = 0.65 (95% CI: 0.46–0.83), difference = 10.28 ± 18.70°].

## 4 Discussions

The main findings of the present study can be summarized as follows: 1. OCT empowered by DL showed substantial agreement with IVUS for calcified plaque detection; 2. The integration of optical properties enabled a refined classification of calcified plaque subtypes and also underscores the reliability of the DL algorithm; 3. The complementary nature of OCT and IVUS was once more demonstrated, setting the preamble for combined IVUS-OCT catheter.

One of the novelties in current study is the precise and comprehensive cross-validation for OCT-DL. Though plaque detection by OCT and IVUS had been previously compared (Wang et al., 2017; Shimokado et al., 2019), the calcifications were still manually identified without implementing any quantitative tissue characterization technologies. To the best of our knowledge, this is the first study attempting to establish a quantitative, objective and comprehensive cross-validation between precisely co-registered OCT and IVUS. The finding of the present study improved our understanding of reality from converging (often) and diverging (sometimes) information sources.

In previous studies, OCT was validated on *ex-vivo* human specimens that have been histologically fixed using conventional methods (Li et al., 2013; Di Vito et al., 2015). After sequences of desiccation, sectioning and alteration by glutaraldehyde, the histomorphometry of specimens tends to be altered, causing significant dimensional changes that might influence interpretation. Some attempts have been made to validate OCT on fresh tissue (Brezinski et al., 1996; Yabushita et al., 2002; Teo et al., 2017). By matching the histology section with OCT images, descriptive definitions for different plaques were proposed and subsequently applied for future analyses (Jang et al., 2002). Using similar methodology, comparisons between OCT and IVUS were performed, and their complementary nature has been repeatedly validated (Jang et al., 2002; Kawasaki et al., 2006; Li et al., 2013; Brown et al., 2015; Nakano et al., 2016).

However, most of these studies were still confined to manual and qualitative interpretations, where calcified plaques were treated as an "all-or-none" variable (Mintz et al., 2001; Tearney et al., 2012; Zeng et al., 2017; Zeng et al., 2018), irrespective of the various patterns of coronary calcification and their progressive nature (Otsuka et al., 2014; Ijichi et al., 2015; Jinnouchi et al., 2020). How to accurately identify and quantify plaques in a more automated and objective way remains an unmet need for interventional cardiologists and biomedical engineers. Several technologies have been developed over the last 15 years (Komiyama et al., 2000; Nair et al., 2002; Bruining et al., 2007; Xu et al., 2008; van Soest et al., 2010; Garcia-Garcia et al., 2011; Athanasiou et al., 2014; Liu et al., 2017; Teo et al., 2017; Villiger et al., 2018; Prabhu et al., 2019; Lee et al., 2020). With the emergence of artificial intelligence, deep learning algorithm provides us with another promising solution. In the present study, by referring to the numerical distribution of optical properties, 95% of the DL-detected calcified plaques were

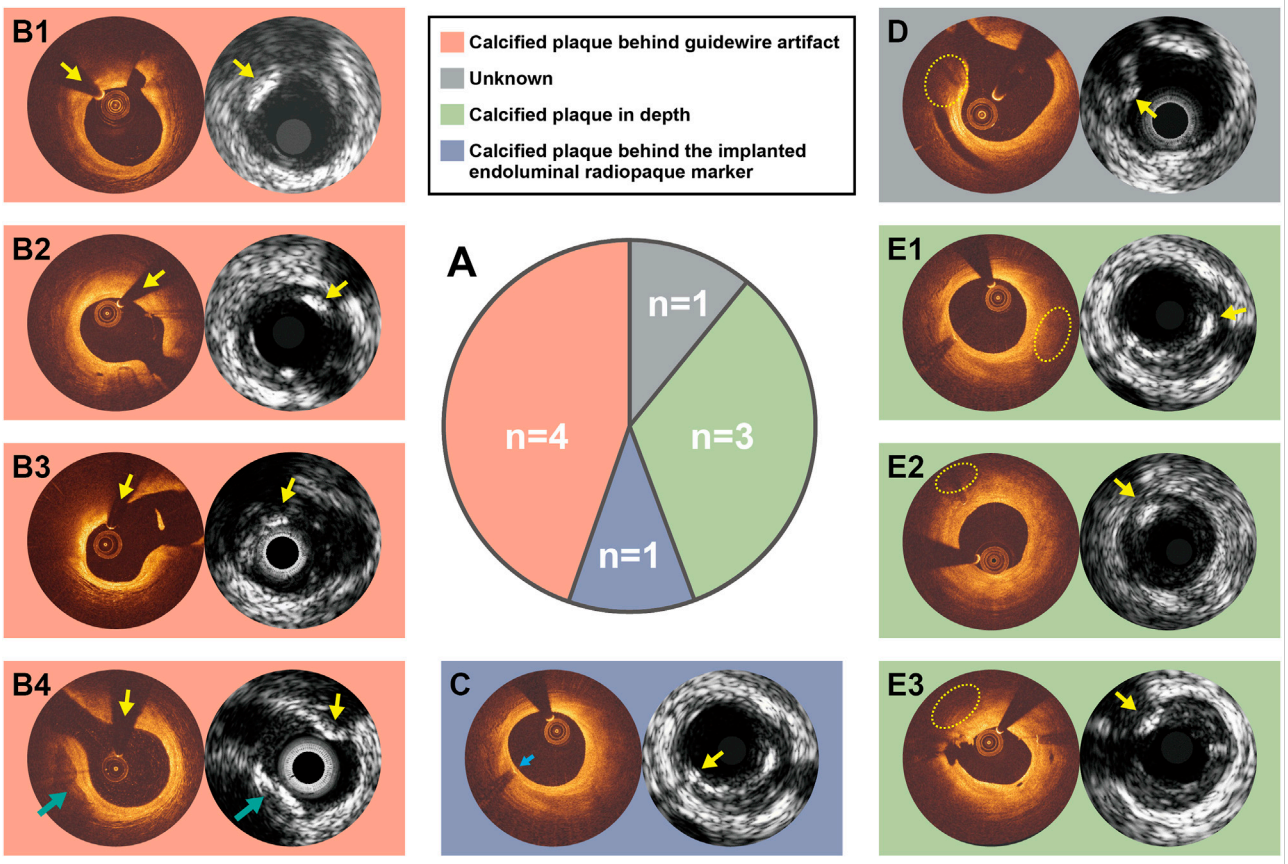


FIGURE 3
Potential explanations for the discordance between OCT and IVUS for calcified plaque identification. Nine calcified plaques were detected by ultrasound signals but not by OCT-DL **(A)**. The discordance between OCT and IVUS for calcified plaque identification might be caused due to calcified plaque behind guidewire artifact **(B1–B4)**, calcified plaque behind the implanted endoluminal platinum marker **(C)**, or calcified plaque in depth **(E1–E3)**. There is one case in which we could not explain the discordance **(D)**. Notably, the calcified plaque at 7-9 o-clock in B4 has been identified by both optical and ultrasound signals (green arrow). C and E1 are of same anatomical slices, where the reasons for discordance are different. Abbreviations as in Figure 1.

TABLE 1 Concordance between OCT-DL and ultrasound signals in calcified plaque identification.

| | Whole population | | After exclusion[a] | |
|---|---|---|---|---|
| | Kappa | Agreement | Kappa | Agreement |
| OCT-DL- GS-IVUS | 0.69 (95% CI: 0.48–0.86) | 90% (95% CI: 82–95%) | 0.77 (95% CI: 0.58–0.91) | 93% (95% CI: 88–97%) |
| OCT-DL- IVUS-VH | 0.60 (95% CI: 0.39–0.77) | 87% (95% CI: 80–92%) | 0.68 (95% CI: 0.49–0.87) | 90% (95% CI: 85–95%) |
| OCT-DL- Echogenicity | 0.60 (95% CI: 0.34–0.78) | 87% (95% CI: 78–92%) | 0.69 (95% CI: 0.49–0.87) | 90% (95% CI: 85–95%) |

[a]Five calcified plaques were excluded since the corresponding areas of IVUS-detected calcified plaques in OCT, were not imaged by the light beam due to the impact of guidewire artifact (n = 4) and implanted endoluminal platinum marker (n = 1).
The bias-corrected 95% CIs, from a bootstrap analysis are reported in brackets, with the patient as cluster and performed 500 replications.
CI: confidence interval; DL: deep learning; GS: greyscale; IVUS: intravascular ultrasound; OCT: optical coherence tomography; VH: virtual histology.

corroborated, underscoring the reliability of this novel method. Meanwhile, refined classification for DL-detected calcified plaque subtypes was also proposed. More pure calcified plaques were observed in the group with perfect optical-ultrasound concordance compared to the ones with partial concordance (76% *versus* 50%), indicating the potential association between

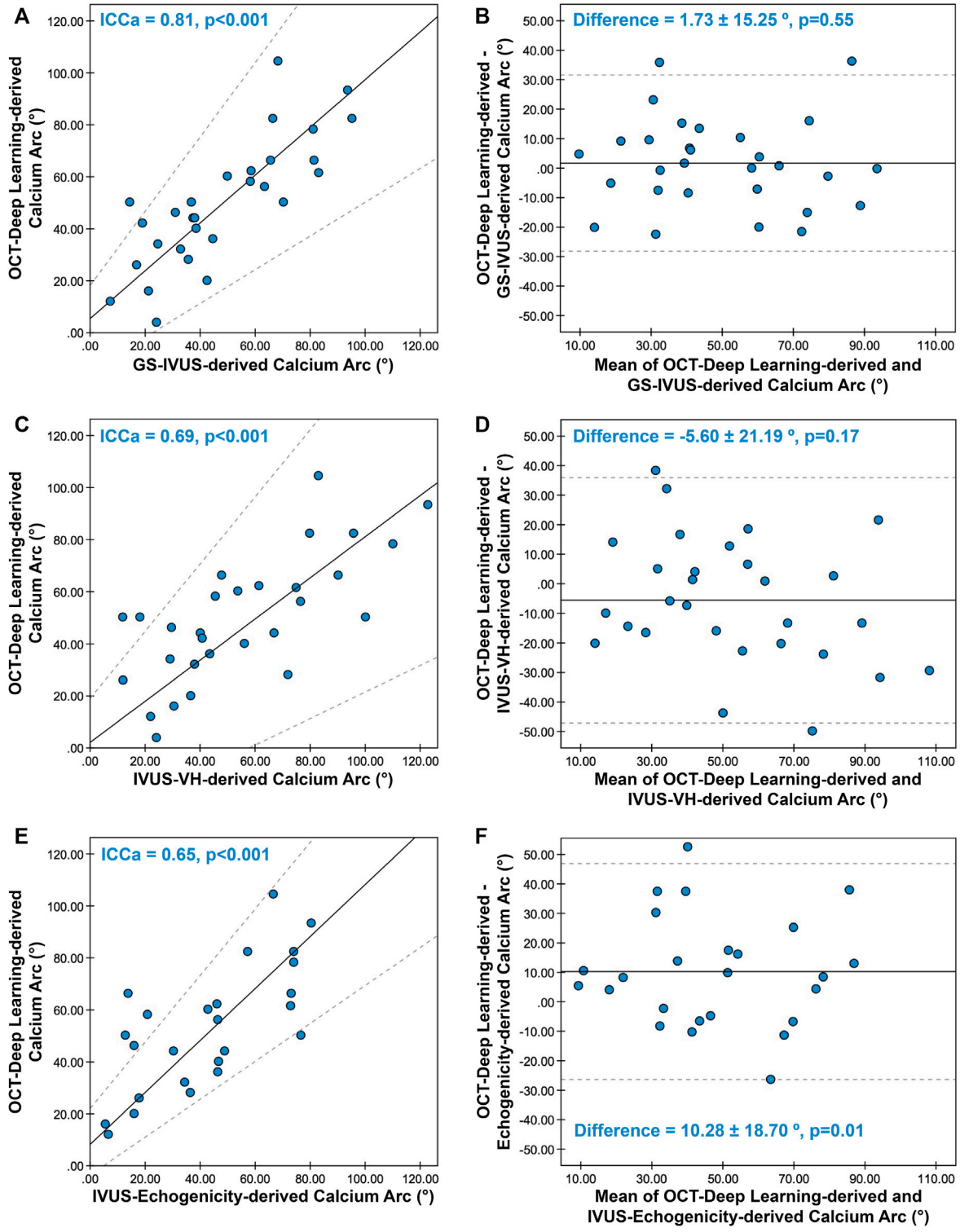


FIGURE 4
Concordance between calcium arc derived from OCT-DL and three ultrasonic imaging modalities. The Passing-Bablok regression and Bland-Altman plot for comparing the calcium arc derived from OCT-DL with GS-IVUS **(A,B)**, IVUS-VH **(C,D)**, and echogenicity **(E,F)**. In A, C, and E, the solid lines and dotted lines correspond to the fitted regression lines and 95% confidence intervals, respectively. In B, D and F, the solid lines and dotted lines correspond to the mean difference and mean difference ±1.96*SD, respectively. GS: greyscale, SD: standard deviation. Other abbreviations as in Figure 1.

calcification patterns and the optical/ultrasound concordance. Future studies are warranted to further investigate the valuable information contained within optical properties, and their potential application in screening out the "false positive" plaques detected by DL.

Although OCT-DL provides an accurate identification for calcified plaques, it will be inevitably impacted by the inherent limitations of OCT including the signal void due to implanted platinum marker or guidewire artifact (Figure 3, Supplementary Figure S4), the latter of which could actually be avoided by withdrawing the guidewire out of the sheath ahead of pullback (Choi et al., 2019; Liu et al., 2020). Of note, the calcium hidden behind the platinum marker and guidewire artifact are of less clinical importance regarding their relatively small size. After excluding the five cases where calcified plaques failed to be imaged due to the above OCT artifactual confounding factors, substantial increase in concordance between optical and ultrasound signals was observed (kappa: 0.69–0.77).

Similar to previous studies, distinctive features of calcified plaque hidden behind areas with significant light attenuation become less apparent on OCT, making it impossible to identify such plaques without prior knowledge (Figure 3, Supplementary Figure S5, Supplementary Table S5). As to IVUS, it was acquired with 20 MHz probes, providing adequate tissue penetration. Though its resolution was not as high as the newly developed high-definition IVUS catheters (Chin et al., 2016), it is still sufficient for calcium detection. In addition, in absence of speckle noise (20 MHz) from blood, the luminal area could be easily delineated, further ensuring the accurate detection of superficial and deep calcified plaques. Of note, the calcium located deeper in the arterial wall or at the interface of media/adventitia is somehow less clinically relevant compared to the one positioned superficially (Virmani et al., 1994; Sugiyama et al., 2019). Thus, the prognostic value of OCT-DL is maintained, regardless of its inferior ability in detecting deep calcium.

Interestingly, we also observed that there were 6 calcified plaques identified by OCT-DL, but not by ultrasound signals (Supplementary Figure S6). Four of these calcified plaques were further corroborated by optical properties (Supplementary Figure S6A,B,C,F). For this reason, we suspected that these 4 DL-detected calcium were not "identified by mistake" but were possibly in early stages of coronary calcification, when the subtle changes in tissue composition were captured by optical signals and observed in OCT images with the features of relatively dense texture and higher than normal backscattering, but not to an extent that could create detectable difference in ultrasound signals. For the resting 2 DL-detected calcified plaques (Supplementary Figure S6D,E), we did not find any supporting findings from other sources. Of note, these two calcified plaques were generally small and whether ultrasound signals were capable of detecting such small calcification remained unknown without histopathologic reference standard. Nevertheless, the presence of such calcifications would be of limited clinical relevance considering their relatively small size and the fact that they only occurred in separated cross-sections.

In addition, there were some discordances within ultrasound signals, among GS-IVUS, IVUS-VH and IVUS-echogenicity for the identification of calcified plaques. A total of 8 anatomic slices showed controversial results. Half of the discordance had calcified plaques identified by both GS-IVUS and IVUS-VH, but not by IVUS-echogenicity (Supplementary Figure S7). In fact, IVUS-echogenicity classifies these 4 calcified plaques as hyperechogenic tissue. A possible explanation for this could be as follows: the signal intensity of these four calcification areas have not reached the numerical threshold in echogenicity algorithm, possibility due to the presence of fibrotic or lipidic components inside the calcification, which lowered the signal intensity of these areas. The resting four anatomic slices have calcified plaques identified by IVUS-VH, but not by GS-IVUS or IVUS-echogenicity (Supplementary Figure S8). These detected calcified plaques were indeed "brighter" than other tissues, which was mainly caused by BRS platinum marker. However, we did not observe any acoustic shadow behind the bright tissue. For this reason, we suspect that IVUS-VH mis-identified these calcified plaques.

In spite of the superb ability of IVUS in identifying deep calcified plaques, the unique interaction between calcium and ultrasound signals, i.e., the acoustic shadow, in turn becomes an obstacle for visualization of tissue hidden behind calcium and prevents precise morphological assessments of calcium area, depth, thickness and volume (Supplementary Table S5). Compared to IVUS, OCT has the valuable capability to "see through the calcium" and to characterize the tissue behind (Kawasaki et al., 2006), provided that the infrared signal reaches the deeper layers of the plaque. Besides, OCT empowered by DL also provides unique value for automated and comprehensive calcium quantification (Supplementary Table S5).

Although the concordance between OCT and IVUS was substantial, we observed a moderate correlation between OCT-derived and IVUS-derived calcium arc. This imperfect concordance was expected since different physical signals providing different spatial resolutions were used. For GS-IVUS, the calcium arc was measured as the arc of the acoustic shadow. In case the calcification is non-confluent with gaps of approximately 100 mm (as is common), part of the ultrasound signal might be able to "pass through" the calcium (Mintz, 2015), leading to the underestimation of the GS-IVUS-derived calcium arc. As a result, the calcium arc measured by OCT-DL was found to be numerically larger than GS-IVUS in current dataset, but statistically insignificant. In

addition, for the purpose of comparability, we measured the calcium arc from the gravitational center of the lumen. However, the location and arc of the acoustic shadow cast by calcified plaques in IVUS tends to be impacted by the catheter location, which emerged as another confounding factor for calcium arc assessment. Nevertheless, due to the lack of "gold standard" and the relatively small sample size in the present study, our current findings may not be sufficient to come up with the conclusion that IVUS underestimates the calcium arc. Future studies with larger dataset, possibly obtained from combined IVUS-OCT catheters, might be able to unravel the numerical concordance between the calcium arcs measured by these two modalities.

## 4.1 Combined IVUS-OCT catheter

The current study once more illustrates the complementary nature of OCT and IVUS. Combined use of these two synergistic, multiparametric imaging modalities demonstrated considerable benefits (Brown et al., 2015). Although providing a comprehensive evaluation, the advantage of incorporating both OCT and IVUS might be partly cancelled by the different cardiac phases during which two pullbacks were performed and the impact of oblique imaging (Supplementary Figure S9). In addition, the length measurement for the same segment also tend to differ between OCT and IVUS pullbacks (Gutierrez-Chico et al., 2012). Most importantly, precise co-registration between OCT and IVUS is usually tedious and time-consuming. Of note, all the above drawbacks could be easily circumvented using combined IVUS-OCT imaging. Up to now, multiple studies have been carried out regarding the development and testing of combined catheters (Li et al., 2013; Alfonso et al., 2021; Leng et al., 2021; Takahashi et al., 2021). The precisely co-registered images and tissue characterization achieved in the present study, on the other hand, provide an example of what would be easily obtainable using combined IVUS-OCT catheters (Supplementary Video S1).

## 4.2 Clinical perspectives

OCT-DL could be applied to any OCT pullbacks without being restricted by the imaging systems. In the near future, the application of combined catheters, once empowered by OCT-DL and image-derived physiological assessment (Huang et al., 2020; Chu et al., 2021; Yu et al., 2021), has the potential to provide precise "3G", namely triple guidance by combining histomorphometry, anatomy and physiological information from single pullback. The comprehensive information provided by combined catheter facilitates a more precise treatment, especially when plaque burden and detailed morphological assessment, such as calcium thickness, failed to be achieved using single modality due to the trade-off between image resolution and signal penetration. The averaged time of OCT-DL analysis was within 30 s for each pullback (Chu et al., 2021), further ensuring its application for real-time assessment in catheterization laboratory. Meanwhile, the precise and automated plaque quantification provided by DL has the potential for guiding and evaluating the effect of plaque modification techniques and PCI procedural strategies.

In addition, the findings in the present study also provide some new insights on future research directions, including the development of a light transparent guidewire eliminating the presence of guidewire artifact in OCT, and the AI-empowered high-frequency IVUS images enabling automated real-time tissue characterization. Besides, the methodology established in the current study for plaque characterization and cross-validation might be further implemented to larger dataset from combined IVUS-OCT catheters for more tissue types including areas infiltrated with foam cells and cholesterol crystals, the latter being closely associated with adverse clinical events (Usui et al., 2021).

## 4.3 Limitations

The current study is limited to 15 patients, which results in wider than desired confidence intervals for some estimations in order to make reliable inferences and a relatively small dataset, the latter is mainly due to the incorporation of electrocardiogram-gated IVUS-VH(Zeng et al., 2017; Zeng et al., 2018). Nevertheless, the precise co-registration utilizing unique BRS platinum markers ensured the quality of current dataset. In addition, the different slice thicknesses of OCT and IVUS might hamper the co-registration accuracy. Therefore, a fixed longitudinal OCT window was applied as a reasonable compromise. Although the calcium classification is refined using optical properties, current trinary interpretation still seems insufficient (Virmani et al., 1994; Otsuka et al., 2014; Jinnouchi et al., 2020). In addition, only calcified plaques were considered for analysis. The findings from the present study may not apply to the identification of calcified nodule, since calcified nodules were not observed in current dataset. Future *ex-vivo* studies are warranted to validate findings derived from these techniques using gold standard, i.e., the histology results. With the development of combined catheters, larger sample sizes could be easily achieved for investigating the interplay between plaque composition and morphology detected by DL on OCT and IVUS corroborated by sophisticated analyses of purely optical and ultrasonic parameters will tell us more about the winning combination of light, sound and spectroscopy. Though the presence of calcification after BRS implantation has been

confirmed by previous histological findings (Von Kossa staining) (Onuma et al., 2010), the potential impact of BRS in optical properties warrant further investigation.

## 5 Conclusion

OCT empowered by deep learning showed substantial agreement with optical and ultrasound signals in detecting coronary calcification. The comprehensive assessment provided by OCT and IVUS heralds the enhanced diagnostic power of combined IVUS-OCT catheters.

## Data availability statement

The dataset can be shared upon reasonable request. Requests to access these datasets should be directed to the corresponding author.

## Author contributions

Conception and design and/or analysis and interpretation of data: PS, YO, WW, JD, and ST. Drafting of the manuscript or revising it critically for important intellectual content: JH, KN, SM, CM, DD, SH, and NO'L. Final approval of the manuscript submitted: PS, YO, WW, JD, and ST.

## Funding

This work was supported in part by grants from the Natural Science Foundation of China (grant numbers: 82020108015 and 81871460) to ST, by the grants from Science Foundation Ireland *via* CÚRAM to PS, and by the grants from Science Foundation Ireland [grant number: 15/RP/2765] to WW, JH, and DD. This publication has emanated from research conducted with the financial support of Science Foundation Ireland under Grant number 15/RP/2765. For the purpose of Open Access, the author has applied a CC BY public copyright license to any Author Accepted Manuscript version arising from this submission.

## Conflict of interest

PS reports personal fees from Sinomedical Sciences Technology, SMT, Philips/Volcano, Novartis, Merillife, and Xeltis. WW reports research grants and honoraria from MicroPort, medical advisor of Rede Optimus Research and co-founder of Argonauts, an innovation facilitator. ST reports research grants and consultancy from Pulse Medical Imaging Technology, outside the submitted work.

The remaining authors declare that the research was conducted in the absence of any commercial or financial relationships that could be construed as a potential conflict of interest.

## Publisher's note



## Supplementary material

The Supplementary Material for this article can be found online at: https://www.frontiersin.org/articles/10.3389/fphot.2022.1019552/full#supplementary-material

**SUPPLEMENTARY VIDEO S1**
Simultaneous co-registration of IVUS and OCT from combined IVUS-OCT catheter. IVUS: intravascular ultrasound; OCT: optical coherence tomography.

## References

Alfonso, F., Del Val, D., and Prati, F. (2021). Comprehensive clinical assessment of coronary plaque phenotype: integrating optical coherence tomography and intravascular ultrasound co-registration. *Coron. Artery Dis.* 33, 125–127. doi:10.1097/MCA.0000000000001104

Athanasiou, L. S., Bourantas, C. V., Rigas, G., Sakellarios, A. I., Exarchos, T. P., Siogkas, P. K., et al. (2014). Methodology for fully automated segmentation and plaque characterization in intracoronary optical coherence tomography images. *J. Biomed. Opt.* 19 (2), 026009. doi:10.1117/1.JBO.19.2.026009

Brezinski, M. E., Tearney, G. J., Bouma, B. E., Izatt, J. A., Hee, M. R., Swanson, E. A., et al. (1996). Optical coherence tomography for optical biopsy. Properties and demonstration of vascular pathology. *Circulation* 93 (6), 1206–1213. doi:10.1161/01.cir.93.6.1206

Brown, A. J., Obaid, D. R., Costopoulos, C., Parker, R. A., Calvert, P. A., Teng, Z., et al. (2015). Direct comparison of virtual-histology intravascular ultrasound and optical coherence tomography imaging for identification of thin-cap fibroatheroma. *Circ. Cardiovasc. Imaging* 8 (10), e003487. doi:10.1161/CIRCIMAGING.115.003487

Bruining, N., Verheye, S., Knaapen, M., Somers, P., Roelandt, J. R., Regar, E., et al. (2007). Three-dimensional and quantitative analysis of atherosclerotic plaque composition by automated differential echogenicity. *Catheter. Cardiovasc. Interv.* 70 (7), 968–978. doi:10.1002/ccd.21310

Chin, C. Y., Maehara, A., Fall, K., Mintz, G. S., and Ali, Z. A. (2016). Imaging comparisons of coregistered native and stented coronary segments by high-definition 60-MHz intravascular ultrasound and optical coherence tomography. *JACC Cardiovasc. Interv.* 9 (12), 1305–1306. doi:10.1016/j.jcin.2016.04.011

Choi, S.-W., Hur, S.-H., Lee, C. H., Cho, Y.-K., Yoon, H.-J., Nam, C.-W., et al. (2019). Optical coherence tomography: Defined plaque erosion after removal of a coronary guidewire. *Korean Circ. J.* 49 (9), 879–881. doi:10.4070/kcj.2019.0088

Chu, M., Jia, H., Gutiérrez-Chico, J. L., Maehara, A., Ali, Z. A., Zeng, X., et al. (2021). Artificial intelligence and optical coherence tomography for the automatic characterisation of human atherosclerotic plaques. *EuroIntervention* 17, 41–50. doi:10.4244/eij-d-20-01355

Di Vito, L., Agozzino, M., Marco, V., Ricciardi, A., Concardi, M., Romagnoli, E., et al. (2015). Identification and quantification of macrophage presence in coronary atherosclerotic plaques by optical coherence tomography. *Eur. Heart J. - Cardiovasc. Imaging* 16 (7), 807–813. doi:10.1093/ehjci/jeu307

Efron, B., and Tibshirani, R. J. (1994). *An introduction to the bootstrap*. Florida: CRC Press.

Garcia-Garcia, H. M., Gogas, B. D., Serruys, P. W., and Bruining, N. (2011). IVUS-based imaging modalities for tissue characterization: similarities and differences. *Int. J. Cardiovasc. Imaging* 27 (2), 215–224. doi:10.1007/s10554-010-9789-7

Gutierrez-Chico, J. L., Serruys, P. W., Girasis, C., Garg, S., Onuma, Y., Brugaletta, S., et al. (2012). Quantitative multi-modality imaging analysis of a fully bioresorbable stent: a head-to-head comparison between QCA, IVUS and OCT. *Int. J. Cardiovasc. Imaging* 28 (3), 467–478. doi:10.1007/s10554-011-9829-y

Huang, J., Emori, H., Ding, D., Kubo, T., Yu, W., Huang, P., et al. (2020). Diagnostic performance of intracoronary optical coherence tomography-based versus angiography-based fractional flow reserve for the evaluation of coronary lesions. *EuroIntervention* 16, 568–576. doi:10.4244/eij-d-19-01034

Ijichi, T., Nakazawa, G., Torii, S., Nakano, M., Yoshikawa, A., Morino, Y., et al. (2015). Evaluation of coronary arterial calcification - *ex-vivo* assessment by optical frequency domain imaging. *Atherosclerosis* 243 (1), 242–247. doi:10.1016/j.atherosclerosis.2015.09.002

Jang, I. K., Bouma, B. E., Kang, D. H., Park, S. J., Park, S. W., Seung, K. B., et al. (2002). Visualization of coronary atherosclerotic plaques in patients using optical coherence tomography: comparison with intravascular ultrasound. *J. Am. Coll. Cardiol.* 39 (4), 604–609. doi:10.1016/s0735-1097(01)01799-5

Jinnouchi, H., Sato, Y., Sakamoto, A., Cornelissen, A., Mori, M., Kawakami, R., et al. (2020). Calcium deposition within coronary atherosclerotic lesion: Implications for plaque stability. *Atherosclerosis* 306, 85–95. doi:10.1016/j.atherosclerosis.2020.05.017

Kawasaki, M., Bouma, B. E., Bressner, J., Houser, S. L., Nadkarni, S. K., MacNeill, B. D., et al. (2006). Diagnostic accuracy of optical coherence tomography and integrated backscatter intravascular ultrasound images for tissue characterization of human coronary plaques. *J. Am. Coll. Cardiol.* 48 (1), 81–88. doi:10.1016/j.jacc.2006.02.062

Komiyama, N., Berry, G. J., Kolz, M. L., Oshima, A., Metz, J. A., Preuss, P., et al. (2000). Tissue characterization of atherosclerotic plaques by intravascular ultrasound radiofrequency signal analysis: an *in vitro* study of human coronary arteries. *Am. Heart J.* 140 (4), 565–574. doi:10.1067/mhj.2000.109217

Lee, J., Prabhu, D., Kolluru, C., Gharaibeh, Y., Zimin, V. N., Dallan, L. A. P., et al. (2020). Fully automated plaque characterization in intravascular OCT images using hybrid convolutional and lumen morphology features. *Sci. Rep.* 10 (1), 2596. doi:10.1038/s41598-020-59315-6

Leng, J., Zhang, J., Li, C., Shu, C., Wang, B., Lin, R., et al. (2021). Multi-spectral intravascular photoacoustic/ultrasound/optical coherence tomography tri-modality system with a fully-integrated 0.9-mm full field-of-view catheter for plaque vulnerability imaging. *Biomed. Opt. Express* 12 (4), 1934–1946. doi:10.1364/BOE.420724

Li, B. H., Leung, A. S., Soong, A., Munding, C. E., Lee, H., Thind, A. S., et al. (2013). Hybrid intravascular ultrasound and optical coherence tomography catheter for imaging of coronary atherosclerosis. *Catheter. Cardiovasc. Interv.* 81 (3), 494–507. doi:10.1002/ccd.24295

Liu, S., Sotomi, Y., Eggermont, J., Nakazawa, G., Torii, S., Ijichi, T., et al. (2017). Tissue characterization with depth-resolved attenuation coefficient and backscatter term in intravascular optical coherence tomography images. *J. Biomed. Opt.* 22 (9), 1–16. doi:10.1117/1.JBO.22.9.096004

Liu, Z., Niu, D., and Guo, J. (2020). Radial artery spiral dissection confirmed by OCT without guidewire shadow. *J. Invasive Cardiol.* 32 (4), E102.

Mintz, G. S., Nissen, S. E., Anderson, W. D., Bailey, S. R., Erbel, R., Fitzgerald, P. J., et al. (2001). American college of cardiology clinical expert consensus document on standards for acquisition, measurement and reporting of intravascular ultrasound studies (IVUS). A report of the American college of cardiology task force on clinical expert consensus documents. *J. Am. Coll. Cardiol.* 37 (5), 1478–1492. doi:10.1016/s0735-1097(01)01175-5

Mintz, G. S. (2015). Intravascular imaging of coronary calcification and its clinical implications. *JACC Cardiovasc. Imaging* 8 (4), 461–471. doi:10.1016/j.jcmg.2015.02.003

Nair, A., Kuban, B. D., Tuzcu, E. M., Schoenhagen, P., Nissen, S. E., and Vince, D. G. (2002). Coronary plaque classification with intravascular ultrasound radiofrequency data analysis. *Circulation* 106 (17), 2200–2206. doi:10.1161/01.cir.0000035654.18341.5e

Nakano, M., Yahagi, K., Yamamoto, H., Taniwaki, M., Otsuka, F., Ladich, E. R., et al. (2016). Additive value of integrated backscatter IVUS for detection of vulnerable plaque by optical frequency domain imaging: An *ex vivo* autopsy study of human coronary arteries. *JACC Cardiovasc. Imaging* 9 (2), 163–172. doi:10.1016/j.jcmg.2015.07.011

Onuma, Y., Serruys, P. W., Perkins, L. E., Okamura, T., Gonzalo, N., Garcia-Garcia, H. M., et al. (2010). Intracoronary optical coherence tomography and histology at 1 month and 2, 3, and 4 years after implantation of everolimus-eluting bioresorbable vascular scaffolds in a porcine coronary artery model: an attempt to decipher the human optical coherence tomography images in the ABSORB trial. *Circulation* 122 (22), 2288–2300. doi:10.1161/CIRCULATIONAHA.109.921528

Otsuka, F., Sakakura, K., Yahagi, K., Joner, M., and Virmani, R. (2014). Has our understanding of calcification in human coronary atherosclerosis progressed? *Arterioscler. Thromb. Vasc. Biol.* 34 (4), 724–736. doi:10.1161/ATVBAHA.113.302642

Prabhu, D. S., Bezerra, H. G., Kolluru, C., Gharaibeh, Y., Mehanna, E., Wu, H., et al. (2019). Automated A-line coronary plaque classification of intravascular optical coherence tomography images using handcrafted features and large datasets. *J. Biomed. Opt.* 24 (10), 1. doi:10.1117/1.jbo.24.10.106002

Serruys, P. W., Onuma, Y., Ormiston, J. A., de Bruyne, B., Regar, E., Dudek, D., et al. (2010). Evaluation of the second generation of a bioresorbable everolimus drug-eluting vascular scaffold for treatment of de novo coronary artery stenosis: six-month clinical and imaging outcomes. *Circulation* 122 (22), 2301–2312. doi:10.1161/CIRCULATIONAHA.110.970772

Shimokado, A., Kubo, T., Matsuo, Y., Ino, Y., Shiono, Y., Shimamura, K., et al. (2019). Imaging assessment and accuracy in coronary artery autopsy: comparison of frequency-domain optical coherence tomography with intravascular ultrasound and histology. *Int. J. Cardiovasc. Imaging* 35 (10), 1785–1790. doi:10.1007/s10554-019-01639-0

Sugiyama, T., Yamamoto, E., Fracassi, F., Lee, H., Yonetsu, T., Kakuta, T., et al. (2019). Calcified plaques in patients with acute coronary syndromes. *JACC Cardiovasc. Interv.* 12 (6), 531–540. doi:10.1016/j.jcin.2018.12.013

Takahashi, T., Latib, A., and Kobayashi, Y. (2021). Complementary assessment by hybrid intravascular ultrasound-optical coherence tomography catheter after implantation of a new-generation drug-eluting stent. *Circ. J.* 85 (11), 2119. doi:10.1253/circj.CJ-21-0318

Tearney, G. J., Regar, E., Akasaka, T., Adriaenssens, T., Barlis, P., Bezerra, H. G., et al. (2012). Consensus standards for acquisition, measurement, and reporting of intravascular optical coherence tomography studies: a report from the international working group for intravascular optical coherence tomography standardization and validation. *J. Am. Coll. Cardiol.* 59 (12), 1058–1072. doi:10.1016/j.jacc.2011.09.079

Teo, J. C., Foin, N., Otsuka, F., Bulluck, H., Fam, J. M., Wong, P., et al. (2017). Optimization of coronary optical coherence tomography imaging using the attenuation-compensated technique: a validation study. *Eur. Heart J. Cardiovasc. Imaging* 18 (8), 880–887. doi:10.1093/ehjci/jew153

Usui, E., Matsumura, M., Mintz, G. S., Zhou, Z., Hada, M., Yamaguchi, M., et al. (2021). Clinical outcomes of low-intensity area without attenuation and cholesterol crystals in non-culprit lesions assessed by optical coherence tomography. *Atherosclerosis* 332, 41–47. doi:10.1016/j.atherosclerosis.2021.08.003

van Soest, G., Goderie, T., Regar, E., Koljenovic, S., van Leenders, G. L., Gonzalo, N., et al. (2010). Atherosclerotic tissue characterization *in vivo* by optical coherence tomography attenuation imaging. *J. Biomed. Opt.* 15 (1), 011105. doi:10.1117/1.3280271

Villiger, M., Otsuka, K., Karanasos, A., Doradla, P., Ren, J., Lippok, N., et al. (2018). Coronary plaque microstructure and composition modify optical polarization: A new endogenous contrast mechanism for optical frequency domain imaging. *JACC Cardiovasc. Imaging* 11 (11), 1666–1676. doi:10.1016/j.jcmg.2017.09.023

Virmani, R., Farb, A., and Burke, A. P. (1994). Coronary angioplasty from the perspective of atherosclerotic plaque: morphologic predictors of immediate success and restenosis. *Am. Heart J.* 127 (1), 163–179. doi:10.1016/0002-8703(94)90522-3

Wang, X., Matsumura, M., Mintz, G. S., Lee, T., Zhang, W., Cao, Y., et al. (2017). *In vivo* calcium detection by comparing optical coherence tomography, intravascular ultrasound, and angiography. *JACC Cardiovasc. Imaging* 10 (8), 869–879. doi:10.1016/j.jcmg.2017.05.014

Xu, C., Schmitt, J. M., Carlier, S. G., and Virmani, R. (2008). Characterization of atherosclerosis plaques by measuring both backscattering and attenuation coefficients in optical coherence tomography. *J. Biomed. Opt.* 13 (3), 034003. doi:10.1117/1.2927464

Yabushita, H., Bouma, B. E., Houser, S. L., Aretz, H. T., Jang, I. K., Schlendorf, K. H., et al. (2002). Characterization of human atherosclerosis by optical coherence tomography. *Circulation* 106 (13), 1640–1645. doi:10.1161/01.cir.0000029927.92825.f6

Yu, W., Tanigaki, T., Ding, D., Wu, P., Du, H., Ling, L., et al. (2021). Accuracy of intravascular ultrasound-based fractional flow reserve in identifying hemodynamic significance of coronary stenosis. *Circ. Cardiovasc. Interv.* 14 (2), e009840. doi:10.1161/CIRCINTERVENTIONS.120.009840

Zeng, Y., Tateishi, H., Cavalcante, R., Tenekecioglu, E., Suwannasom, P., Sotomi, Y., et al. (2017). Serial assessment of tissue precursors and progression of coronary calcification analyzed by fusion of IVUS and OCT: 5-Year follow-up of scaffolded and nonscaffolded arteries. *JACC Cardiovasc. Imaging* 10 (10), 1151–1161. doi:10.1016/j.jcmg.2016.11.016

Zeng, Y. P., Cavalcante, R., Collet, C., Tenekecioglu, E., Sotomi, Y., Miyazaki, Y., et al. (2018). Coronary calcification as a mechanism of plaque/media shrinkage in vessels treated with bioresorbable vascular scaffold: a multimodality intracoronary imaging study. *Atherosclerosis* 269, 6–13. doi:10.1016/j.atherosclerosis.2017.11.002